**Proceedings of the ASME 2016 Dynamic Systems and Control Conference**
**DSCC2016**
**October 12-14, 2016, Minneapolis, MN, USA**

# PRELIMINARY INVESTIGATION OF PROVABILITY OF LI-ION MACROSCALE MODELS SUBJECT TO CAPACITY FADE

**Harikesh Arunachalam**
Department of Automotive Engineering
Clemson University
Greenville, South Carolina 29607
Email: harunac@clemson.edu

**Ilenia Battiato**
Department of Mechanical Engineering
San Diego State University
San Diego, California 92182
Email: ibattiato@mail.sdsu.edu

**Simona Onori**
Department of Automotive Engineering
Department of Electrical and Computer Engineering
Clemson University
Greenville, South Carolina 29607
Email: sonori@clemson.edu

## ABSTRACT

*Estimating the remaining useful life of lithium-ion batteries is crucial for their application as energy storage devices in stationary and automotive applications. It is therefore important to understand battery degradation based on chemistry, usage patterns, and operating environment. Different degradation mechanisms that affect performance and durability of lithium-ion batteries have been identified over the past decades. Amongst them, the solid-electrolyte interface (SEI) layer growth has been observed to be the most influential cause of capacity fading. In this paper, we introduce for the very first time, a framework that evaluates the predictive ability of physics-based macroscopic models in capturing battery dynamics as function of their state-of-health (SoH). Using data from accelerated aging experiments, we identify the applicability conditions of classical electrochemical models. This analysis is performed using a phase diagram approach that involves parameters controlling the micro-scale dynamics inside the lithium-ion cell.*

## Introduction

A comprehensive understanding of the dynamic performance of lithium-ion batteries over the duration of its useful life still remains a significant challenge today. Non-linearity of the transport processes within the battery system, coupled with physicochemical heterogeneities over a multiplicity of length scales makes this task very complex [1]. As batteries age, their performance degrades due to capacity and power fading. Capacity fade is referred to the loss of cyclable lithium ions as a result of electrode degradation caused by the reversible transfer of lithium ions during battery operation [2]. This leads to loss of energy storage capacity in the electrodes. Lithium-ion batteries age differently as a consequence of their operating patterns. This utilization behavior will greatly determine the amount of capacity fading due to cyclic aging, and the eventual end of life of the battery [3].

Among the different aging mechanisms, the growth of the SEI layer has been observed to significantly impact battery capacity [4]. Many studies have identified this growth at the anode based on galvanostatic [5, 6] and dynamic operating conditions [7]. During cycling, the SEI layer forms between the anode and electrolyte. Initially, this layer acts as a protective barrier, allowing lithium ion transfer while keeping the electrolyte separated physically from the anode. The continued growth that occurs during cycling will increase the resistive layer and remove active lithium from the cycling system. Gradually, this leads to diminishing energy and power capacity of the battery.

The SEI layer growth can be coupled with existing battery macroscopic models to simulate capacity fade occurring throughout the cell. The rate of the side reactions and the growth of the SEI layer are dependent on the local overpotentials and internal concentrations. These factors directly depend on the battery operating conditions (state-of-charge (SoC), temperature, and C-rate). While this approach has been widely im-

plemented [8–10], the ability of models in predicting battery dynamic performance is something that has not been explored. This is important for the development of advanced algorithms in battery management system (BMS) applications.

In our previous work [11], a homogenized electrochemical model was developed to describe mass and charge transport in lithium-ion batteries. The upscaling methodology enables the quantification of lithium transport mechanisms using phase diagrams in the electrode and electrolyte. Our subsequent work [12] examined the temperature-influenced dynamics of different lithium-ion battery cathodes. This study determined the range of applicability of classical macroscopic models [13], and identified temperature and C-rate of operation as critical parameters that govern the internal transport processes. The outcome of this analysis elucidates the need for multi-scale models for operating conditions where macroscopic models are invalidated.

The novel contribution of this paper is evaluating the ability of macroscopic models in predicting the performance of lithium-ion battery cells as function of their state-of-health (SoH). In the next section, we summarize the applicability conditions of macroscale transport equations in the electrolyte. In the subsequent section, we present the methodology to determine dimensionless micro-scale transport parameters as a function of aging. In the penultimate section, we investigate the effect of SEI layer growth on the applicability conditions of macroscale transport models in the electrolyte. An analytical study of moderate and aggressive battery galvanostatic discharge as a function of the battery SoH is presented. The final section summarizes the conclusion of this work and the direction of future research.

## Applicability conditions of lithium transport in the electrolyte

The pore-scale transport mechanisms of lithium in the electrolyte are heterogeneous reaction, ion diffusion, and ion electro-migration. A time-scale is associated with each of these mechanisms: $\hat{t}_R$ for reaction, $\hat{t}_{D_e}$ for diffusion, and $\hat{t}_{M_e}$ for electro-migration. We identify dimensionless transport numbers, Damköhler $Da_e$ and Péclet $Pe_e$, as parameters that control lithium-ion transport processes. We refer the reader to [11] for the derivation and elaborate explanation of these parameters. They are defined as the ratio of time scales of lithium transport processes [11]:

$$Da_e = \frac{\hat{t}_{D_e}}{\hat{t}_R} = \frac{Lk}{FD^e} = \varepsilon^{\beta}, \quad Pe_e = \frac{\hat{t}_{D_e}}{\hat{t}_{M_e}} = \frac{RTK^e}{D^e F^2 c^s_{max,n}} = \varepsilon^{-\alpha}. \tag{1}$$

In (1), $\varepsilon$ is the ratio of characteristic length scales of the pore-scale and macroscale domains, $L$ is the macroscopic length scale, $k$ the electrochemical reaction rate constant, $F$ Faraday's constant, $R$ the universal gas constant, $T$ temperature, and $c^s_{max,n}$ the maximum lithium storage concentration in the active particle. $D^e$ and $K^e$ are the characteristic values of interdiffusion and electric conductivity in the electrolyte. Parameters $\alpha$ and $\beta$ determine the system behavior in the electrolyte phase.

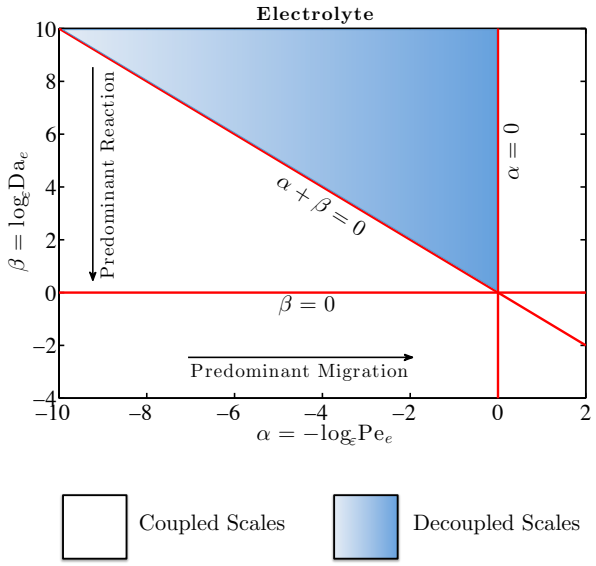


***FIGURE 1**: Phase diagram specifying the range of applicability of macroscopic mass and charge transport equations of lithium-ions in the electrolyte. This figure has been reproduced from [11].*

Upon homogenization [11], rigorous upscaling of the pore-scale mass and charge transport equation is achieved. It is guaranteed that pore-scale lithium-ion transport in the electrolyte is accurately represented by macroscopic equations within errors of order $\varepsilon^2$, provided the following conditions are satisfied:

(a) $Da_e < 1 \Longleftrightarrow \beta > 0$ ,
(b) $Pe_e < 1 \Longleftrightarrow \alpha < 0$, and
(c) $Da_e/Pe_e < 1 \Longleftrightarrow \alpha + \beta > 0$.

Figure 2 schematically represent these conditions in the form of a phase diagram. The shaded portion of the phase diagram (in blue) represents the region where the three constraints are satisfied, which allows the decoupling of the pore-scale and the macroscale equations of lithium transport. Constraints (a) to (c) require that both interface reaction and electro-migration have slower dynamics compared to electrolyte diffusion. This guarantees uniform distribution of lithium-ions at the pore-scale. In diffusion-limited regimes (for instance, at high C-rates of operation), the system is not well-mixed and concentration gradients form at the pore-scale. The predictive ability of continuum scale models can no longer be guaranteed when this occurs. In the subsequent sections, we investigate the effect of aging based on

SEI layer growth to determine if mass transport limitations occur in the electrolyte lithium transport.

### Micro-scale transport parameters as a function of aging

The capacity fade study in our approach is based upon has been developed in [14]. The evolution of the SEI layer at the anode surface in [14] is based on solvent diffusion and single particle approximation [15]. A lumped parameter approach is used to describe the variation in the negative electrode porosity. No active material deformation is considered, and the loss of cyclic lithium ions is the main capacity loss mechanism. Assuming the loss of battery capacity $Q$ is exclusively due to the loss of cyclable Li-ions in the negative electrode due to the side reaction after de-lithiation, then [14]

$$\frac{dQ}{dt} = S_n \cdot i_s, \tag{2}$$

where $S_n$ is the electroactive surface area of the negative electrode and $i_s$ is the current density of the side-reaction leading to the formation of the SEI layer. $S_n$ is related to the geometrical parameters of the electrode as [14]

$$S_n = 3 \cdot \eta_{s,n} \cdot \delta_n \cdot A / R_{s,n}. \tag{3}$$

In (3), $\eta_{s,n}$ is the anode porosity, $\delta_n$ is the thickness of the anode, $A$ is the anode cross-sectional area, and $R_{s,n}$ is the radius of the anode active particle. The growth rate of the SEI layer can be expressed using the current density of the SEI layer side-reaction current, [14]

$$\frac{\delta_{SEI}}{dt} = -\frac{i_s}{2F} \cdot \frac{M_{SEI}}{\rho_{SEI}}, \tag{4}$$

with $M_{SEI}$ the molar mass of the SEI layer, $\rho_{SEI}$ the density of the SEI layer. Combining (2), (3), and (4), we postulate an expression for the SEI layer as a function of time as

$$\delta_{SEI,t} = \delta_{SEI,0} + \frac{M_{SEI}}{2 \cdot F \cdot S_n \cdot \rho_{SEI}} \cdot (Q_0 - Q_t) \tag{5}$$

where $\delta_{SEI,0}$ and $Q_0$ are the initial SEI layer thickness and capacity, and $\delta_{SEI,t}$ and $Q_t$ are the SEI layer thickness and capacity at a later time $t > 0$. (5) is postulated based on the knowledge of the initial SEI layer thickness. In most cases, as indicated in [14], this value is estimated. The battery capacity is determined by considering that the anode provides all the cyclic lithium ions that travel across the electrolyte to the cathode. Assuming discharge conditions, $Q_t$ is expressed in terms of the discharge current, $I_{discharge}$, and the time at the beginning and end of discharge, $t_0$ and $t_f$, respectively as follows,

$$Q_t = \int_{t_0}^{t_f} I_{discharge} \cdot dt \tag{6}$$

$Q_t$ can be expressed in terms of the maximum lithium-ion concentration in the anode, $c^s_{max,n,t}$, as [14]

$$Q_t = \eta_{s,n} \cdot z_n \cdot c^s_{max,n,t} \cdot A \cdot L_n \cdot F \cdot \left(x_{100\%,n} - x_{0\%,n}\right). \tag{7}$$

In (7), $z_n$ is the anode valence number, $x_{100\%,n}$ is the stoichiometric coefficient at 100% SoC, and $x_{0\%,n}$ is the stoichiometric coefficient at 0% SoC. The value of $c^s_{max,n,t}$ as a function of aging can be determined by equating the cell capacity from the assessment tests in the expression for $Q_t$.

The effective electrolyte conductivity, $K^{eff}_{e,n}$, decreases due to cell aging according to the following relationship, due to the growth of the SEI layer thickness at the outer surface of the anode active material, [14]

$$K^{eff}_{e,n} = K^e \cdot \left\{1 - \eta_{f,n} - \eta_{s,n}\left(1 + \frac{3\delta_{SEI,t}}{R_{s,n}}\right)\right\}^{1.5} \tag{8}$$

In the above expression, $\eta_{f,n}$ is the porosity of the filler material in the anode, and $K^e$ is the electrolyte conductivity in the microscale. The power factor of 1.5 is obtained by incorporating the Bruggeman relationship to determine the effective (macroscopic) conductivity in the electrolyte as a function of its microscopic counterpart [14]. We postulate an expression for the microscopic electrolyte conductivity $K^e_{ag}$, in which the aging effect is incorporated using the relationship below

$$K^{eff}_{e,n} = K^e_{ag} \cdot (\eta_{e,n})^{1.5} \tag{9}$$

To the best of our knowledge, no description has been reported in literature on the impact of SEI layer growth on pore-scale parameters. Since their impact on effective transport parameters has been described in [14], we incorporate this information in our postulated expression (9). Combining (8) and (9),

$$K^e_{ag} = \frac{K^e}{(\eta_{e,n})^{1.5}} \cdot \left\{1 - \eta_{f,n} - \eta_{s,n}\left(1 + \frac{3\delta_{SEI,t}}{R_{s,n}}\right)\right\}^{1.5}. \tag{10}$$

Similarly, a parameter $D^e_{ag}$ is postulated for the electrolyte diffusion as a function of aging. The effective electrolyte diffusivity of lithium ions in the anode, $D^{eff}_{e,n}$, decreases due to cell aging as: [14]

$$D^{eff}_{e,n} = D^e \cdot \left\{1 - \eta_{f,n} - \eta_{s,n}\left(1 + \frac{3\delta_{SEI,t}}{R_{s,n}}\right)\right\}^{1.5}. \quad (11)$$

Therefore, the microscopic electrolyte diffusion $D^e_{ag}$ which incorporates the effect of the SEI layer growth (aging) is

$$D^e_{ag} = \frac{D^e}{(\eta_{e,n})^{1.5}} \cdot \left\{1 - \eta_{f,n} - \eta_{s,n}\left(1 + \frac{3\delta_{SEI,t}}{R_{s,n}}\right)\right\}^{1.5}. \quad (12)$$

For isothermal macroscopic models which do not incorporate aging effects, we define the microscopic transport parameters in which the effect of aging is incorporated, as shown above using (10) and (12). We can now define the Damköhler and Péclet numbers below, respectively, in the electrolyte as a function of the aging parameters

$$Da_e = \frac{Lk}{FD^e_{ag}} = \frac{Lk}{FD^e} \cdot \frac{(\eta_{e,n})^{1.5}}{\left\{1 - \eta_{f,n} - \eta_{s,n}\left(1 + \frac{3\delta_{SEI,t}}{R_{s,n}}\right)\right\}^{1.5}}, \quad (13)$$

$$Pe_e = \frac{RTK^e_{ag}}{D^e_{ag}F^2c^s_{max,n,t}} = \frac{RTK^e}{D^eF^2c^s_{max,n,t}}. \quad (14)$$

In the next section, we analyze the impact of the SEI layer growth on the dimensionless transport parameters and their influence on the applicability conditions.

## Battery dynamics as a function of aging

The phase diagram analysis has been until now [11, 12] implemented to study the robustness of macroscopic models at a given state of health. This study focuses on evaluating the ability of macroscopic models to predict the behavior of battery cells as they age. Data for this study is obtained from [16]. Accelerated aging experimental tests were conducted on lithium-ion pouch cells of blended cathodes NMC-LMO (nickel-manganese-cobalt oxide-lithium manganese dioxide). Intermittent cell characterization tests (capacity test in discharge, and hybrid power pulse characterization (HPPC)) were conducted to assess the energy and power capability of these cells as a function of their SoH. We use data from these capacity tests for our analysis.

In this paper, we make the following assumptions:

1. The effect of the relaxation phase of the pulse train event on the growth of the SEI layer is negligible compared to the positive and negative pulse events during cyclic aging.
2. The assessment tests conducted for cell characterization have minimal impact on the SEI layer growth compared to the accelerated aging experiment.
3. The SEI layer is formed only at the anode during charging/discharging events, and is assumed to uniformly grow at the outer surface of the active anode particle.

The target application for the lithium-ion pouch cells analyzed in this study is plug-in hybrid electric vehicles (PHEVs), which operate under charge-depleting (CD) and charge-sustaining modes (CS). The power demand of the CD and CS micro-cycles described in [16] indicates that the pouch-cell under investigation operates in discharge mode between C-rates of 1 and 10. We conduct a phase diagram analysis for two current rates of galvanostatic discharge of the pouch cell: 1 C-rate (moderate) and 10 C-rate (high). The galvanostatic discharge is considered to begin with a battery SoC of 100%. This analysis is used to evaluate model predictability when the cell is tested at two different health conditions: 100% SoH (fresh) and 86% SoH (aged).

Model parameters used to assess the veracity of macroscale models as a function of the pouch cell SoH were obtained from [17–19]. This analysis investigates the impact of C-rate of operation, temperature, and SoH on the micro-scale transport parameters ($k$, $D^e$, and $K^e$). The reaction rate constant at room temperature ($T_{ref}$ = 298K) is determined from the current demand $I_{app}$ using the expression

$$I_{app} = 2 \cdot k_{ref} \cdot \sqrt{\hat{c}^e_\varepsilon \hat{c}^s_\varepsilon \left(1 - \frac{\hat{c}^s_\varepsilon}{c^s_{max}}\right)} \cdot \sinh[F(\hat{\phi}^s_\varepsilon - \hat{\phi}^e_\varepsilon - \hat{U})/2RT_{ref}], \quad (15)$$

where $c^e_\varepsilon$ and $c^s_\varepsilon$ represent the concentration of lithium-ion in the electrolyte and active particles, respectively. The stoichiometric coefficient $x$ is used to determine the value of $c^s_\varepsilon$ from the cell SoC and $c^s_{max}$. We set the value of $c^e_\varepsilon$ as 1,000 mol/m$^3$. The parameters $\phi^s_\varepsilon$, $\phi^e_\varepsilon$, and $\hat{U}$ are respectively the electrode potential, electrolyte potential, and the open-circuit potential. The parameter $(\hat{\phi}^s_\varepsilon - \hat{\phi}^e_\varepsilon - \hat{U})$ is also known as the overpotential, whose value is taken as 100mV [19] for this analysis. The scale separation parameter $\varepsilon = \frac{2R_{s,n}}{L}$ is the ratio of the anode particle diameter ($25\mu$m) and anode thickness ($162\mu$m).

In order to determine $Da_e$ as a function of aging, $k$ must be determined as $c^s_{max,n,t}$ decreases with the SEI layer growth. Assuming galvanostatic discharge at the anode, we can determine the anode reaction rate constant $k_{ref,n}$. Table (1) presents the values of $k_{ref,n}$ determined as a function of the C-rate of discharge and $c^s_{max,n,t}$. Table (2) summarizes the results of the capacity

***TABLE 2**: Lithium-ion pouch cell parameters determined from capacity fading analysis.*

| Ah-throughput [kAh] | $Q_t$ [Ah] | SoH [%] | $\delta_{SEI,t}$ [m] | $c^s_{max,n,t}$ [mol/m$^3$] | $D^e_{ag}$ [m$^2$/s] | $K^e_{ag}$ [$\Omega^{-1}$m$^{-1}$] |
|---|---|---|---|---|---|---|
| 0 | 14.98 | 100 | 0 | 31,833 | 2e-10 | 0.56 |
| 3.1 | 14.36 | 95.9 | 2.09e-7 | 30,516 | 1.83e-10 | 0.51 |
| 4.7 | 14.27 | 95.3 | 2.40e-7 | 30,325 | 1.8e-10 | 0.51 |
| 8.5 | 13.96 | 93.2 | 3.44e-7 | 29,666 | 1.72e-10 | 0.48 |
| 12.8 | 13.87 | 92.6 | 3.75e-7 | 29,475 | 1.7e-10 | 0.48 |
| 17.5 | 13.34 | 89.1 | 5.53e-7 | 28,349 | 1.56e-10 | 0.44 |
| 21 | 13.13 | 87.7 | 6.24e-7 | 27,903 | 1.5e-10 | 0.42 |
| 21.3 | 12.94 | 86.4 | 6.88e-7 | 27,499 | 1.46e-10 | 0.41 |

***TABLE 3**: Variation of the electrolyte phase diagram parameters for different C-rate and temperature, as a function of their SoH.*

| SoH [%] | C-rate [1/h] | $\varepsilon$ [-] | $k$ [A·m·mol$^{-1}$] | T [K] | $D^e_{ag}$ [m$^2$sec$^{-1}$] | $K^e_{ag}$ [$\Omega^{-1}$m$^{-1}$] | Da$_e$ [-] | Pe$_e$ [-] | $\alpha$ [-] | $\beta$ [-] |
|---|---|---|---|---|---|---|---|---|---|---|
| 100 | 1 | 0.154 | 1.94e-4 | 298 | 2e-10 | 0.56 | 1.63e-3 | 2.34e-2 | -2.01 | 3.44 |
| 100 | 1 | 0.154 | 2.39e-4 | 300 | 2.14e-10 | 0.61 | 1.88e-3 | 2.40e-2 | -2.00 | 3.36 |
| 100 | 1 | 0.154 | 2.95e-4 | 302 | 2.28e-10 | 0.66 | 2.17e-3 | 2.45e-2 | -1.98 | 3.28 |
| 100 | 1 | 0.154 | 3.62e-4 | 304 | 2.42e-10 | 0.71 | 2.51e-3 | 2.50e-2 | -1.97 | 3.20 |
| 100 | 1 | 0.154 | 4.43e-4 | 306 | 2.56e-10 | 0.76 | 2.90e-3 | 2.55e-2 | -1.96 | 3.13 |
| 86.4 | 1 | 0.154 | 2.09e-4 | 298 | 1.45e-10 | 0.406 | 2.41e-3 | 2.71e-2 | -1.93 | 3.22 |
| 86.4 | 1 | 0.154 | 2.57e-4 | 300 | 1.59e-10 | 0.456 | 2.72e-3 | 2.79e-2 | -1.91 | 3.16 |
| 86.4 | 1 | 0.154 | 3.17e-4 | 302 | 1.73e-10 | 0.506 | 3.08e-3 | 2.87e-2 | -1.90 | 3.10 |
| 86.4 | 1 | 0.154 | 3.89e-4 | 304 | 1.87e-10 | 0.556 | 3.49e-3 | 2.94e-2 | -1.89 | 3.03 |
| 86.4 | 1 | 0.154 | 4.76e-4 | 306 | 2.01e-10 | 0.606 | 3.98e-3 | 3.00e-2 | -1.88 | 2.96 |
| 100 | 10 | 0.154 | 1.94e-3 | 298 | 2e-10 | 0.56 | 1.63e-2 | 2.34e-2 | -2.01 | 2.20 |
| 100 | 10 | 0.154 | 3.26e-3 | 303 | 2.35e-10 | 0.685 | 2.33e-2 | 2.48e-2 | -1.98 | 2.01 |
| 100 | 10 | 0.154 | 8.79e-3 | 313 | 3.04e-10 | 0.93 | 4.86e-2 | 2.69e-2 | -1.94 | 1.62 |
| 100 | 10 | 0.154 | 2.23e-2 | 323 | 3.73e-10 | 1.17 | 1e-1 | 2.84e-2 | -1.91 | 1.23 |
| 100 | 10 | 0.154 | 5.35e-2 | 333 | 4.42e-10 | 1.42 | 2.03e-1 | 3e-2 | -1.88 | 0.85 |
| 86.4 | 10 | 0.154 | 2.08e-3 | 298 | 1.45e-10 | 0.406 | 2.41e-2 | 2.71e-2 | -1.93 | 1.99 |
| 86.4 | 10 | 0.154 | 3.51e-3 | 303 | 1.80e-10 | 0.53 | 3.27e-2 | 2.90e-2 | -1.90 | 1.83 |
| 86.4 | 10 | 0.154 | 9.46e-3 | 313 | 2.49e-10 | 0.77 | 6.38e-2 | 3.14e-2 | -1.85 | 1.47 |
| 86.4 | 10 | 0.154 | 2.40e-2 | 323 | 3.19e-10 | 1.02 | 1.26e-1 | 3.35e-2 | -1.82 | 1.11 |
| 86.4 | 10 | 0.154 | 5.76e-2 | 333 | 3.88e-10 | 1.26 | 2.49e-1 | 3.51e-2 | -1.79 | 0.74 |

fading analysis performed on the lithium-ion pouch cell. Using this information, we determine the variation of the phase diagram parameters ($\alpha$,$\beta$) for galvanostatic discharge at 1 C-rate and 10 C-rate for a fresh pouch-cell (SoH = 100%) and an aged pouch-cell (SoH = 86%). Based on prior experimental data [19–22] and assuming the discharge to begin at an initial cell temperature of 298K, we estimate the temperature increase to be respectively 298K to 306K for 1 C-rate discharge and 298K to 333K for 10

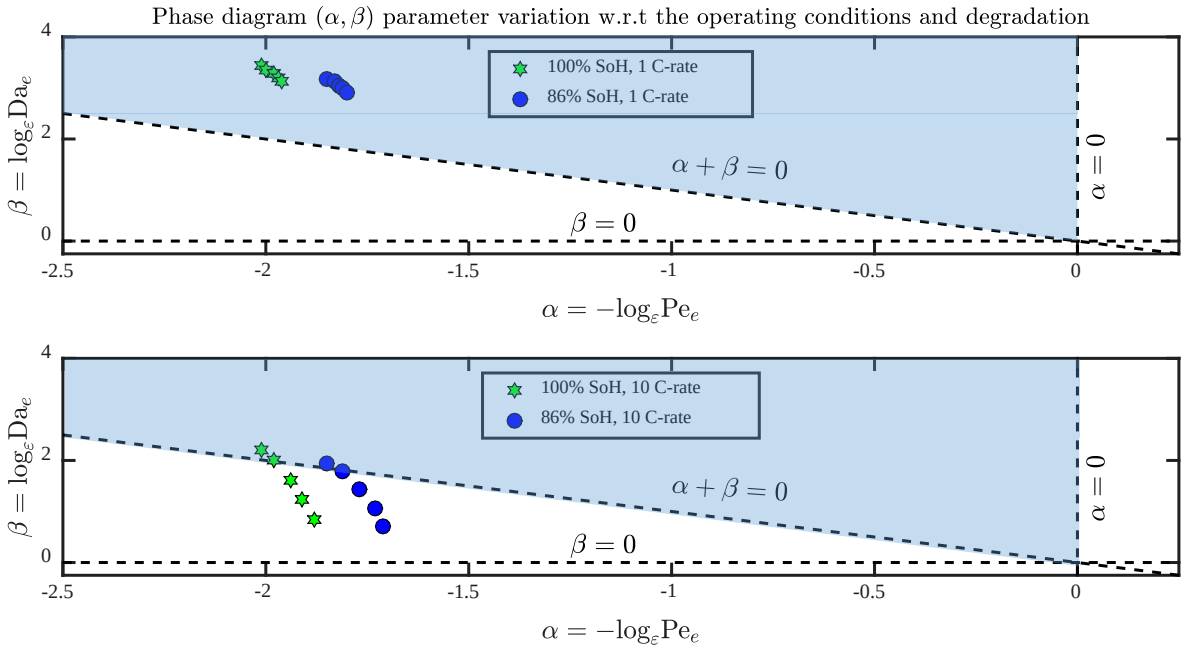


***FIGURE 2**: Variation with temperature of dimensionless parameters α and β for galvanostatic discharge at 1 and 10 C-rates, with the performance evaluated at 100% and 86% SoH.*

***TABLE 1**: Reference reaction rate constant $k_{ref,n}$ in terms of the applied current $I_{app}$ as a function of its SoH and C-rate.*

| SoH [%] | $c^s_{max,n,t}$ [mol/m$^3$] | C-rate [1/h] | $I_{app}$ [A/m$^2$] | $k_{ref,n}$ [A·m/mol] |
|---|---|---|---|---|
| 100 | 31,833 | 1 | 2.84 | 1.94e-4 |
| 86.4 | 27,499 | 1 | 2.84 | 2.09e-4 |
| 100 | 31,833 | 10 | 28.4 | 1.94e-3 |
| 86.4 | 27,499 | 10 | 28.4 | 2.08e-3 |

C-rate discharge.

The electrochemical transport parameters $k$, $D^e$, and $K^e$ also vary as a function of temperature. For the reaction rate constant, we can express $k(T)$ using the Arrhenius relationship [23]:

$$k(T) = k_{ref} \cdot \exp\left[\frac{Ea_r}{R}\left(\frac{1}{T_{ref}} - \frac{1}{T}\right)\right]. \tag{16}$$

$Ea_r$ is the electrode reaction rate activation energy, and we set it to a value of 78.24 kJ/mol [24]. To the best of our knowledge, no analytical dependence has been reported in literature. We implement instead a curve fitting procedure based on Figures 13 and 14 in [25] to determine $D^e(T)$ and $K^e(T)$. This method has earlier been succesfully implemented in [12].

Based on the parameter values reported above and the methodology described earlier, we compute the temperature dependent trajectory of the phase diagram coefficients ($\alpha$,$\beta$) at different temperature intervals that are characteristic of the C-rate of operation and the cell SoH. The variation of parameters $\alpha$ and $\beta$ as a function of the operating conditions are presented in Table (3). This variation is also schematically represented in Figure 2.

At a 1 C-rate, moderate increase in temperature during the discharge event results in a minor change in the parameter $\alpha$ compared to $\beta$. This is due to the faster rate of increase in reaction kinetics compared to the enhanced electrolyte diffusion and conductivity. The effect of cell operation at different SoH can be clearly observed in both parameters, as lower SoH pushes the parameter values closer to the boundary of the applicability regime (indicated by the dotted lines in figure 2). In both cases, the data points satisfy the constraints over the range of temperature increase. Hence macroscale transport models would be capable of capturing pore-scale dynamics accurately.

During 10 C-rate of discharge, significant increase in battery internal temperature leads to an accelerated decrease in $\beta$. The effect of increasing $k$ dominates any increase in parameters $D^e$ and $K^e$. The condition $\alpha + \beta > 0$ is violated shortly after discharge begins. This is because fast reaction kinetic lead to the formation of diffusion-limited regimes. Such poorly mixed conditions leads to the lack of scale separation between the pore-scale and macroscale domains. Operating aged cells under aggressive conditions of discharge has a significant effect on the

trajectory of $(\alpha,\beta)$. The data points for aged cell tend to violate the conditions of homogenizability faster, as shown in figure 2. Lower SoH battery operation lead the points closer to the limiting boundaries and invalidate macroscale models.

The proposed theory suggests that the predictive ability of macroscale models degrade as the battery SoH decreases over time. This is consistent with previous experimental/numerical studies, and can be explained by variation of the parameters $Da_e$ and $Pe_e$ as a function of aging using the applicability conditions:

1. The Péclet number $Pe_e$ increases with aging due to the decrease in battery capacity $Q_t$, which leads to a decrease in $c^s_{max,n,t}$.
2. The Damkhöler number $Da_e$ increases with aging due to the decrease in $D^e_{ag}$, which is the result of the SEI formation side-reaction.
3. The ratio of the Damkhöler and Péclet number, $Da_e/Pe_e$, increases with aging and is directly proportional to the ratio $\frac{c^s_{max,n,t}}{\left\{1-\eta_{f,n}-\eta_{s,n}\left(1+\frac{3\delta_{SEI}}{R_{s,n}}\right)\right\}^{1.5}}$.

In addition, decreasing $c^s_{max,n,t}$ leads to an increase in the rate constant $k_{ref,n}$ for the same current demand as the cell ages. As explained in [15], the applied current determines the total current density at the negative electrode. The total current density is a sum of the intercalation and the side-reaction current densities. As the growth of the SEI layer depletes cyclable lithium ions and increases the unwanted side-reaction dynamics, the intercalation current density must compensate for these losses in order to meet the current demand. As a result, we observe increase in the intercalation side-reaction kinetics. The successful implementation of the phase diagram approach can identify when classical macroscopic models may fail to accurately capture battery dynamics with respect to degradation.

## Conclusions

Understanding the predictive ability of macroscale lithium-ion battery models is essential for the design of algorithms to prolong battery life. This becomes even more crucial as the batteries age over time, and control algorithms must be modified according to the evolution of battery dynamics. The core contribution of this paper was to develop a framework that provides insight as to how well physics-based models today may perform throughout the useful life of a battery.

We performed an aging analysis to determine the dimensionless Damkhöler and Péclet numbers in the electrolyte phase as a function of operating conditions and aging. This study incorporated the impact of SEI layer growth on the surface of anode active particles. The phase diagram analysis helps in understanding the ability of macroscale models to capture battery dynamics under different operating conditions and SoH.

We infer that the predictive ability of macroscale models degrades with battery aging due to the side-reaction dynamics that affects pore-scale transport. The applicability conditions provide a quantitative framework to identify the onset of mass transport limitations as the battery SoH decreases over time. Under such circumstances, modeling efforts must be focused on the implementation of coupled micro-macro models, which can offer better fidelity due to their ability to inherently incorporate microstructural electrode details.

Future studies will focus on the numerical simulation of macroscale models to validate the analytical results presented in this work. In addition to the SEI layer growth, we will assess the impact of other aging mechanisms such as lithium plating and lithium dendrite formation on pore-scale dynamics, and extend the scope of this research work.

## REFERENCES


[1] Pistoia, G., 2014. *Lithium Ion Batteries Advances and Applications*. Elsevier, Oxford.

[2] Vetter, J., Novak, P., Wagner, M. R., Veit, C., Möller, K.-C., Besenhard, J. O., Winter, M., Wohlfahrt-Mehrens, M., Vogler, C., and Hammouche, A., 2005. "Ageing mechanisms in lithium-ion batteries". *J. Power Sources,* ***147***, pp. 269–281.

[3] Barré, A., Deguilhem, B., Grolleau, S., Gérard, M., Suard, F., and Riu, D., 2013. "A review on lithium-ion battery ageing mechanisms and estimations for automotive applications". *J. Power Sources,* ***241***, pp. 680–689.

[4] Pinson, M. B., and Bazant, M. Z., 2013. "Theory of SEI Formation in Rechargeable Batteries: Capacity Fade, Accelerated Aging and Lifetime Prediction". *J. Electrochem. Soc,* ***160***(2), pp. A243–A250.

[5] Ramadass, P., Haran, B., Gomadam, P. M., White, R. E., and Popov, B. N., 2004. "Development of First Principles Capacity Fade Model for Li-Ion Cells". *J. Electrochem. Soc,* ***151***(2), pp. A196–A203.

[6] Liu, P., Wang, J., Garner, J. H., Sherman, E., Soukiazian, S., Verbrugge, M., Tataria, H., Musser, J., and Finamore, P., 2010. "Aging Mechanisms of LiFePO4 Batteries Deduced by Electrochemical and Structural Analyses". *J. Electrochem. Soc,* ***157***(4), pp. A499–A507.

[7] Lawder, M. T., Northrop, P. W. C., and Subramanian, V. R., 2014. "Model-Based SEI Layer Growth and Capacity Fade Analysis for EV and PHEV Batteries and Drive Cycles". *J. Electrochem. Soc,* ***161***(14), pp. A2099–A2108.

[8] Christensen, J., and Newman, J., 2004. "A Mathematical Model for the Lithium-Ion Negative Electrode Solid Electrolyte Interphase". *J. Electrochem. Soc,* ***151***(11), pp. A1977–A1988.

[9] Prasad, G. K., and Rahn, C. D., 2013. "Model based iden-

tification of aging parameters in lithium ion batteries". *J. Power Sources,* ***232***, pp. 79–85.

[10] Awarke, A., Pischinger, P., and Ogrzewalla, J., 2013. "Pseudo 3D Modeling and Analysis of the SEI Growth Distribution in Large Format Li-Ion Polymer Pouch Cells". *J. Electrochem. Soc,* ***160***(1), pp. A172–A181.

[11] Arunachalam, H., Onori, S., and Battiato, I., 2015. "On Veracity of Macroscopic Lithium-Ion Battery Models". *J. Electrochem. Soc,* ***162***(10), pp. A1940–A1951.

[12] Arunachalam, H., Onori, S., and Battiato, I., 2015. "Temperature-dependent multiscale-dynamics in Lithium-ion battery electrochemical models". In Proceedings of the 2015 American Control Conference, pp. 305–310.

[13] Doyle, M., Fuller, T. F., and Newman, J., 1993. "Modeling of Galvanostatic Charge and Discharge of the Lithium/Polymer/Insertion Cell". *J. Electrochem. Soc,* ***140***(6), pp. 1526–1533.

[14] Prada, E., Domenico, D. D., Creff, Y., Bernard, J., S-Moynot, V., and Huet, F., 2013. "A Simplified Electrochemical and Thermal Aging Model of LiFePO4-Graphite Li-ion Batteries: Power and Capacity Fade Simulations". *J. Electrochem. Soc,* ***160***(4), pp. A616–A628.

[15] Ning, G., and Popov, B. N., 2004. "Cycle Life Modeling of Lithium-Ion Batteries". *J. Electrochem. Soc,* ***151***(10), pp. A1584–A1591.

[16] Arenas, A. C., Onori, S., Guezennec, Y., and Rizzoni, G., 2015. "Capacity and power fade cycle-life model for plug-in hybrid electric vehicle lithium-ion battery cells containing blended spinel and layered-oxide positive electrodes". *J. Power Sources,* ***278***, pp. 473–483.

[17] Kumaresan, K., Guo, Q., Ramadass, P., and White, R. E., 2006. "Cycle life performance of lithium-ion pouch cells". *J. Power Sources,* ***158***, pp. 679–688.

[18] Kumaresan, K., Sikha, G., and White, R. E., 2008. "Thermal Model for a Li-Ion Cell". *J. Electrochem. Soc,* ***155***(2), pp. A164–A171.

[19] Guo, M., Sikha, G., and White, R. E., 2011. "Single Particle Model for a Lithium-Ion Cell: Thermal Behavior". *J. Electrochem. Soc,* ***158***(2), pp. A122–A132.

[20] Ye, Y., Shi, Y., and Tay, A. A. O., 2012. "Electro-thermal cycle life model for lithium iron phosphate battery". *J. Power Sources,* ***217***, pp. 509–518.

[21] Baba, N., Yoshida, H., Nagaoka, M., Okuda, C., and Kawauchi, S., 2014. "Numerical simulation of thermal behavior of lithium-ion secondary batteries using the enhanced single particle model". *J. Power Sources,* ***252***, pp. 214–228.

[22] Gambhire, P., Hariharan, K. S., Khandelwal, A., Kolake, S. M., Yeo, T., and Doo, S., 2014. "A physics based reduced order aging model for lithium-ion cells with phase change". *J. Power Sources,* ***270***, pp. 281–291.

[23] Guo, M., and White, R. E., 2011. "Thermal Model for Lithium Ion Battery Pack with Mixed Parallel and Series Combination". *J. Electrochem. Soc,* ***158***(10), pp. A1166–A1176.

[24] Park, J., Seo, J. H., Plett, G., Lu, W., and Sastry, A. M., 2011. "Numerical Simulation of the Effect of the Dissolution of LiMn2O4 Particles on Li-Ion Battery Performance". *J. Electrochem. Soc,* ***14***(12), pp. A14–A18.

[25] Valoen, L. O., and Reimers, J. N., 2005. "Transport Properties of LiPF6-Based Li-Ion Battery Electrolytes". *J. Electrochem. Soc,* ***152***(5), pp. A882–A891.